

# EXPERIMENTAL QUANTIFICATION OF DROPLET COLLISION RATES IN TURBULENT SPRAYS

**Róbert Bordás, Thomas Hagemeier and Dominique Thévenin**  
Laboratory of Fluid Dynamics & Technical Flows  
University of Magdeburg "Otto von Guericke"  
Universitätsplatz 2, 39106 Magdeburg, Germany  
bordas@ovgu.de, hagemeier@ovgu.de, thevenin@ovgu.de

## ABSTRACT

In this publication, droplet collision rates in turbulent sprays are quantified experimentally. It is documented in the scientific literature that the presently employed theoretical models underestimate the influence of turbulence on the collision rates. The discrepancy between theory and measurements will be quantified here by a direct comparison between measured and predicted collision rates considering different turbulent properties and droplet size distributions.

The present paper describes in detail the corresponding procedure, starting with a description of the experimental facility, and then introducing how to measure the collision rates in turbulent sprays. Two different measurement configurations are considered and corresponding parameters are listed. The results obtained from the measurements are then presented, together with a comparison using appropriate theoretical approaches for each configuration. Finally, conclusions are drawn and the importance of measurement data to clarify this issue is discussed.

## INTRODUCTION

Collision rates of water droplets found in turbulent sprays are a key property to understand many practical issues, e.g., for accurate numerical predictions of vehicle soiling by rain (Hagemeier et al., 2011), or of warm rain initiation in cumulus clouds (Bordás et al., 2010b). Many theoretical (for instance Dodin and Elperin (2002)) and numerical (for instance Pinsky et al. (2008)) studies are available in the literature concerning this issue, but reliable experimental data concerning droplet-droplet interactions in turbulent flows with controlled conditions can hardly be found. Developing a suitable experimental database is the central purpose of the present project, allowing finally model testing and improvement by direct comparisons between theory and measurements.

For the experimental investigations of collisions, Shadowgraphy is applied, which is an established imaging measurement method. In this way, droplet velocity and diameter distributions are measured. One advantage of Shadowgraphy compared to other non-intrusive measurement methods is that it is able to directly observe collision events.

In a previous work (Bordás et al., 2010a), it has been

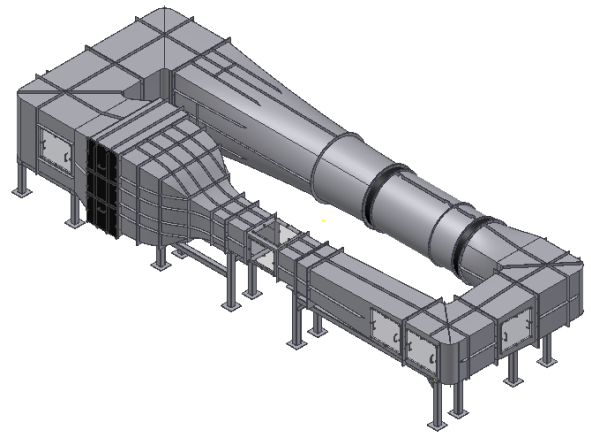


Figure 1. Two-phase wind tunnel employed for this study.

demonstrated that Shadowgraphy can be indeed applied for a quantitative investigation of collision processes in dilute sprays. However, only the collision probability (number of collisions divided by the number of droplets) can be directly obtained from the measurement technique discussed in Bordás et al. (2010a). For a quantification of the collision rate (number of collisions per unit volume and time), the droplet rate per unit volume is required as well, which is acquired separately using Phase-Doppler Anemometry (PDA).

The structure of this paper is arranged as follows: first, the experimental facility used to measure the collision rates in turbulent sprays is described. The two different measurement configurations are introduced together with corresponding parameters. The results obtained from the measurements are then presented and compared with appropriate theoretical approaches for each configuration. Conclusions and perspectives are finally proposed.

## EXPERIMENTAL FACILITY

All experimental measurements take place in the two-phase wind tunnel with a transparent measurement section available at the University of Magdeburg (Fig. 1). The ve-



Figure 2. Close view of the spray heads and injected sprays (left: small droplets, Case 1; right: large droplets, Case 2).

locity of the air flow averaged over the cross section was varied from 2.32 m/s to 2.92 m/s (in Case 1) and from 15 up to 25 m/s (in Case 2). The two configurations considered are distinguished as follows:

Case 1: Small droplets moving at moderate air velocities with inhomogeneous droplet concentration distributions, as found for example in cumulus clouds (Bordás et al., 2010b).

Case 2: Large droplets, driven by high wind velocities and therefore inhomogeneously distributed, as encountered for instance when considering rain at ground level (Hagemeier et al., 2011).

### Case 1: small droplets

This configuration is specifically tailored to investigate warm rain initiation (Bordás et al., 2010b). Small droplets in cumulus clouds move typically with moderate air velocities. During the wind tunnel experiments, representative mean velocities between 2.32 m/s and 2.92 m/s are employed. These values are set by prescribing a constant rotation speed of the fan with the help of the frequency regulator of the wind tunnel. The mean turbulent kinetic energy of the flow was measured to be between 0.18 m<sup>2</sup>/s<sup>2</sup> and 0.22 m<sup>2</sup>/s<sup>2</sup> (Bordás et al., 2010b), since the spray head and the counter-flow injection of the water droplets (Fig. 2) generated relatively high velocity fluctuations. In addition, a cylindrical bluff body with a diameter of 20 mm was mounted horizontally at a height of  $z = 90$  mm, perpendicular to the main flow direction, in order to produce large-scale coherent structures and inhomogeneities in droplet number density. In the measurement case with 2.92 m/s air flow velocity, a passive grid with a rectangular grid size of 25 mm was additionally mounted. Water droplets were generated by air-assisted full-cone pneumatic atomizing nozzles (166.208.16.12 and 154.104.16.14, respectively, from the Co. Lechler, Germany; see Fig. 2, left), applying an air gauge pressure of 1.2 bar and 2.0 bar, respectively, with a mean droplet size around  $d_{10} = 10$  μm. To keep the inlet values constant, a PID-controller was programmed. In this way, it was possible to obtain a steady water volume flow rate leading to constant droplet properties during the whole acquisition time. The typically obtained droplet size distribution can be described by a probability density function as a two-parameter log-normal distribution,

$$y = f(d|\mu, \sigma) = \frac{1}{d\sigma\sqrt{2\pi}} \exp\left[-\frac{(\ln(d) - \mu)^2}{2\sigma^2}\right], \quad (1)$$

with the shape and scale parameters  $\sigma = 0.72$  and  $\mu = 2.41$  respectively.

The collision probability was measured in a single plane ( $x = 0$  mm), 620 mm downstream of the spray head, at different positions along the vertical center line, for both previously mentioned nozzles, beginning in the middle of the cross-section ( $z = 0$  mm), down to 140 mm. Since different turbulent properties were measured in the flow at these various locations (as shown later in Table 1), the impact of varying turbulent conditions on the measured collision rate can be assessed in this manner.

### Case 2: large droplets

The second experimental configuration employed higher cross-section mean velocities of 15, 20 and 25 m/s, set in the same manner as described previously. The turbulence properties in terms of turbulent kinetic energy of the flow were measured as well and found to be in the range of 0.71 m<sup>2</sup>/s<sup>2</sup> (at 15 m/s), 1.32 m<sup>2</sup>/s<sup>2</sup> (20 m/s) and 2.34 m<sup>2</sup>/s<sup>2</sup> (at 25 m/s). Contrary to the previous configuration, the spray head is now injecting in co-flow direction. This leads to higher slip velocities between the ambient air flow and the droplets and, even more significant, to an inhomogeneous droplet distribution in the test section of the wind tunnel. To generate the spray a single orifice, flat cone, pressure injector (CJM type from Co. Delavan) was used, working at a gauge pressure of 0.3 bar with a flow rate of 5.4 l/min.

A multimodal distribution was obtained by means of PDA measurements for the droplet size distribution, as shown in Fig. 3.

In Case 2, the turbulence is not modified by any grid or bluff body. Due to the large size of those droplets, they would anyway respond only very slowly to corresponding fluctuations. The influence of turbulent conditions is hence varied only through the different wind speeds in this configuration.

Moreover, the effect of the gravitational force is much more significant for the large droplets of Case 2. The residence time of the droplets within the test section is conditioned by the air velocity. A higher air velocity leads to a smaller residence time and therefore to a smaller terminal velocity in gravitational direction. This terminal velocity is a decisive quantity for droplet collision rates when considering large droplets.

For Case 2, the collision probability was measured only at a single position,  $(x, y, z) = (0, 0, 0)$  mm, 570 mm behind the spray head. This is due to the fact that the spray droplets are highly concentrated and rapidly thin out for positions at increased distance from the central axis. Moreover, the droplets within the spray cone center are somewhat smaller than at the edges and can be detected with higher accuracy using PDA. The turbulence properties are varied by changing the air flow velocity, yielding three parameter sets.

### Measurement method

Shadowgraphy, employed here to quantify droplet-droplet interactions, is an imaging measurement method, relying typically on a CCD-camera, a far-field microscope, and a pulsed laser with a fluorescence disc. The camera and the illumination lie on the same optical axis. As the droplets are illuminated from behind, their shadow image is recorded on

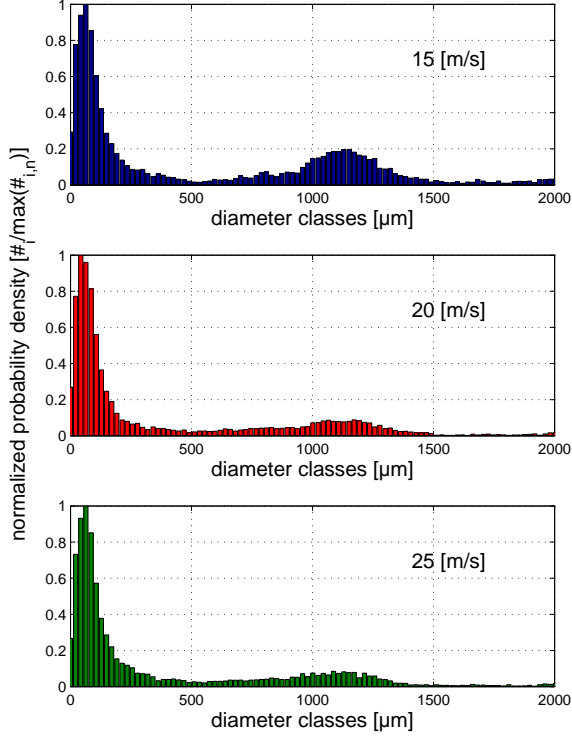


Figure 3. Droplet size distribution (DSD) for Case 2 at three different mean air velocities (15, 20 and 25 m/s).

the camera and the diameter of the droplets can be obtained by means of a previously calibrated  $\mu\text{m}/\text{pix}$  value (Bordás et al., 2006; Kapulla et al., 2007). As the expected collision rate is usually moderate in dispersed flows, and since the recording frequency of the camera is limited to 10 Hz, measurements with meaningful statistics must be carried out for a long period of time at a chosen position. The collision events are then identified automatically, using a threshold value for the centrality values. Finally, the number of collisions is divided by the total number of evaluated droplets in order to get the collision probability. A detailed description of the image processing algorithm and postprocessing calculation steps is given in Bordás et al. (2010a).

## RESULTS

The applied evaluation algorithm is based on droplet shape recognition and discriminates collision events from aerodynamic droplet deformation, which is an essential issue when considering large droplet diameters as in Case 2. On the contrary, the measurements of Case 1 rely on a flow configuration with almost uniform mean droplet diameter but with spatially varying velocity fluctuations due to the bluff-body, leading locally to interesting variations in number density values (Shaw et al., 1998) together with turbulent properties.

The properties needed to compute later the collision rates are summarized in Table 1 for Case 1 and in Table 3 for Case

Table 1. Properties required for the calculation of collision rates at the discussed measurement points (Case 1), as measured by PDA.

	$d_{10}$ [ $\mu\text{m}$ ]	$n$ [ $1/\text{m}^3$ ]	$u'_{p,rel}$ [ $\text{m/s}$ ]
Nozzle no. 166.208.16.12			
$z = 0$	14.50	5.74e+9	0.31
$z = 40$	14.20	5.50e+9	0.36
$z = 90$	13.70	6.83e+9	0.43
$z = 140$	14.00	4.74e+9	0.33
Nozzle no. 154.104.16.14			
$z = 0$	9.70	2.57e+9	0.22
$z = 20$	10.10	2.31e+9	0.23
$z = 40$	9.70	2.59e+9	0.25
$z = 60$	9.60	2.31e+9	0.40
$z = 90$	8.05	3.21e+9	0.67
$z = 120$	7.50	2.40e+9	0.61
$z = 140$	7.75	1.92e+9	0.40

2.

## Theoretical collision rate

For comparison with theory, different established models can be found in the literature, from which the most suitable ones were selected for the corresponding conditions.

**Case 1: Small droplets** For Case 1, the droplet collision rate is obtained following Williams and Crane (1983):

$$N = n^2 d^2 \left( 8\pi \overline{u_{p,rel}^2} \right)^{1/2}, \quad (2)$$

for a mono-disperse distribution, where  $N$  is the number of collisions per unit volume and unit time,  $n$  is the number of droplets per unit volume, with a mean diameter  $d_{10}$  and the variance of the relative droplet velocities in the mean flow direction is  $\overline{u_{p,rel}^2}$ . The theoretical collision rate was calculated by the above equation for each size class pair obtained by discretizing the distribution with a resolution of  $1 \mu\text{m}$ :

$$N = \sum_{i,j} N_{i,j} = \sum_{i,j} n_i n_j d_i d_j \left( 8\pi (u_{i,p,rel}^2 + u_{j,p,rel}^2) \right)^{1/2}. \quad (3)$$

Due to symmetry ( $N_{i,j} = N_{j,i}$ ), only half of the matrix has to be considered. Finally, the elements of one triangular part of

the resulting matrix (see Eq. 4) were then summed up, to consider each collision event exactly once (including the matrix principal diagonal).

An identical procedure was used to estimate the collision rate of the second experimental configuration using the same discretization step of 1  $\mu\text{m}$ , which was found appropriate for this case as well. The influence of the discretization step size has been checked by varying its value and observing the associated convergence (Richardson extrapolation).

$$N_{i,j} = \begin{pmatrix} n_{1,1} & n_{1,2} & n_{1,3} & \dots & n_{1,j} \\ - & n_{2,2} & n_{2,3} & \dots & n_{2,j} \\ - & - & n_{3,3} & \dots & n_{3,j} \\ \vdots & \vdots & \vdots & \dots & \vdots \\ - & - & - & \dots & n_{i,j} \end{pmatrix} \quad (4)$$

The theoretical droplet collision rates calculated in this manner are presented in the first column (entitled Theory) of Table 2 and 4, respectively for small and large droplets. For comparison with them, collision rates  $N$  estimated experimentally by Shadowgraphy following the procedure described in Bordás et al. (2010a) are also listed. The experimental collision rate has been determined in two different manners: either using the data rate (subscript  $D$ , collision rate  $N_D$ ) or the concentration (subscript  $C$ , data rate  $N_C$ ) respectively, both obtained from PDA measurements. The two results are nearly identical, confirming the robustness of the procedure. Furthermore, the standard deviation associated with the experimental measure of the collision rates is given in the Tables as  $\sigma$ .

**Large droplets** Another theoretical model can be found in the literature (Abrahamson, 1975), more suitable for large droplets, when particle motion is uncorrelated with the fluid flow (large Stokes numbers  $\text{Stk} \rightarrow \infty$ ). It also takes into account body forces. Since gravity has a major impact on larger droplets, the formulation for particle collisions taking into account gravity is retained here to compare with the corresponding experimental configuration. According to Abrahamson (1975) the collision rate for a binary collision is given as:

$$N = n_1 n_2 d_1 d_2 \pi \text{abs}(\mathbf{u}_1 - \mathbf{u}_2), \quad (5)$$

yielding a collision probability ranging from 0.387 to 0.674 % for the present conditions of Case 2. The quantities appearing in this equation are the number of collisions per unit volume  $N$ , the number of droplets per unit volume  $n$ , the droplet diameter  $d$  and the relative velocity of the colliding droplets  $\mathbf{u}$ . In the present case the vectorial droplet velocity  $\mathbf{u}$  is considered to consist of only two dimensions, the main flow direction of the wind tunnel and the vertical direction. The transverse flow is not known and has been thus neglected. However, complementary measurements of the transverse velocity component by Particle Image Velocimetry (PIV) revealed that this is at least an order of magnitude smaller than the velocity components in the measurement plane.

It should be kept in mind that the previous equation is only valid for binary collisions and not for a broad droplet size

Table 3. Properties required for the calculation of collision rates (Case 2), as measured by PDA.

	$d_{10}$ [ $\mu\text{m}$ ]	$n$ [ $1/\text{m}^3$ ]	$u'_{p,rel}$ [ $\text{m/s}$ ]
$v = 15$ m/s	594	2.986e+6	2.076
$v = 20$ m/s	413	6.801e+6	2.296
$v = 25$ m/s	398	1.089e+7	2.950

distribution. For collisions of droplets associated to various size classes, as is the case in our applications and particularly for Case 2, the equation is hence reformulated as:

$$N = \sum_{i,j} N_{i,j} = \sum_{i,j} n_i n_j d_i d_j \pi \text{abs}(\mathbf{u}_i - \mathbf{u}_j). \quad (6)$$

In Table 4 the results obtained from the measurements and the predictions from theory are compared. As can be seen, there is a slight deviation whether the number of droplets per unit volume is calculated from the measured droplet concentration ( $N_C$ ) or from the observed data rate ( $N_D$ ). However, this difference is negligible compared to the discrepancy observed between theoretical predictions and measured collision rates. All experimental results lead to much higher collision rates, from 29 up to 80 times the theoretically expected value for the present conditions.

## DISCUSSION

The measured collision rates are systematically higher than the theoretical predictions. For Case 1 (small droplets), both values are nevertheless quite close to each other and show the same order of magnitude. The difference is still noticeable, typically a factor of 2 to 5, and would be sufficient to explain the apparent difficulty in predicting warm rain initiation using current models. Somewhat surprisingly, the difference appears to be even higher for larger droplets. In Case 2, a difference by a factor of typically 50 is found compared to theory. Even if the real distributions have been completely taken into account in the analysis, this might be due to the complex DSD found in Case 2 compared to Case 1, involving collision partners of very different size. On-going, systematic measurements involving in particular a wider range of volume fractions are clearly needed before drawing general conclusions concerning the accuracy of the models and of the measurements.

A summary of the experimental results involving both Case 1 and Case 2 is presented in Figure 4, where the collision probability is plotted as function of the droplet volume fraction (note the log scales). As expected, the collision probability increases with increasing volume fraction. Similar tendencies are observed for the ratio of the experimental and theoretical collision rates. In a first attempt, a simple linear fit of the experimental data has been computed to determine the corresponding correlation. The results of this fit are shown in Figure 4 together with the correlation quality  $R^2$ . The obtained exponents are very similar. However, it is clearly es-

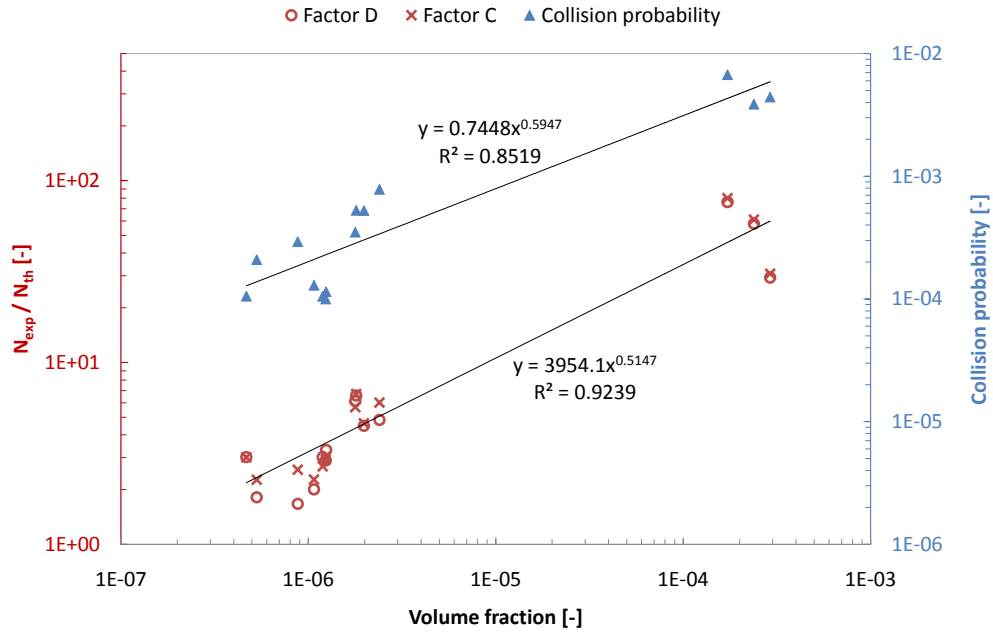


Figure 4. Ratio of collision rates (experiment/theory involving red symbols, left) and collision probability (blue symbols, right) versus droplet volume fraction.

Table 2. Collision rates in  $1/m^3s$  for Case 1 together with standard deviation  $\sigma$ , and comparison with theoretical predictions.

Location	Theory	$N_D$	$\sigma_{N,D}$	$N_C$	$\sigma_{N,C}$	$\frac{N_D}{Theory}$	$\frac{N_C}{Theory}$
Nozzle no. 154.104.16.14							
$z = 0$	9.66e+9	4.33e+10	3.84e+9	4.47e+10	7.05e+9	4.49	4.63
$z = 40$	6.77e+9	4.44e+10	3.81e+9	4.52e+10	6.89e+9	6.59	6.71
$z = 90$	1.26e+10	6.07e+10	4.10e+9	7.56e+10	9.10e+9	4.83	6.02
$z = 140$	5.22e+9	3.20e+10	3.85e+9	2.96e+10	6.34e+9	6.14	5.68
Nozzle no. 166.208.16.12							
$z = 0$	1.85e+9	5.58e+9	6.32e+8	4.96e+9	5.56e+8	3.02	2.68
$z = 20$	1.66e+9	5.48e+9	7.02e+8	5.05e+9	6.40e+8	3.30	3.05
$z = 40$	1.72e+9	4.97e+9	6.40e+8	5.02e+9	6.40e+8	2.89	2.92
$z = 60$	2.68e+9	5.37e+9	8.64e+8	6.08e+9	9.67e+8	2.01	2.27
$z = 90$	6.62e+9	1.11e+10	1.98e+9	1.70e+10	2.99e+9	1.67	2.57
$z = 120$	4.28e+9	7.75e+9	1.21e+9	9.70e+9	1.49e+9	1.81	2.27
$z = 140$	1.37e+9	4.12e+9	6.53e+8	4.11e+9	6.40e+8	3.02	3.01

sential to obtain further measurements in the intermediate region of volume fraction before discussing these correlations in more details.

## ACKNOWLEDGEMENTS

This project is part of the federative research project SPP 1276 - MetStroem funded by the German Research Foundation (DFG). Corresponding financial support is warmly acknowledged here.

Table 4. Collision rates in  $1/\text{m}^3\text{s}$  for Case 2 with standard deviation  $\sigma$ , and comparison with theoretical predictions.

Exp. configuration	Theory	$N_D$	$\sigma_{N,D}$	$N_C$	$\sigma_{N,C}$	$\frac{N_D}{\text{Theory}}$	$\frac{N_C}{\text{Theory}}$
$v = 15 \text{ m/s}$	1.06e+7	8.08e+8	1.87e+8	8.49e+8	1.88e+8	76	80
$v = 20 \text{ m/s}$	2.88e+7	1.67e+9	3.99e+8	1.76e+9	3.99e+8	58	61
$v = 25 \text{ m/s}$	1.04e+8	3.05e+9	7.08e+8	3.20e+9	7.08e+8	29	31

## REFERENCES

- J. Abrahamson. Collision rates of small particles in a vigorously turbulent fluid. *Chemical Engineering Science*, 30: 1371–1379, 1975.
- R. Bordás, A. Öncül, K. Zähringer, and D. Thévenin. Optical measurements in two-phase flows involving particles. In G. Kompenhans and A. Schröder, editors, *12th International Symposium on Flow Visualization*, pages 025/1–10, Göttingen, Germany, 2006.
- R. Bordás, T. Hagemeier, and D. Thévenin. Experimental investigation of droplet-droplet interactions. In *23rd European Conference on Liquid Atomization and Spray Systems*, pages 198.1–6, Brno, Czech Republic, 2010a.
- R. Bordás, T. Hagemeier, B. Wunderlich, and D. Thévenin. Droplet collisions and interaction with the turbulent flow within a two-phase wind tunnel. *Physics of Fluids*, submitted for publication, 2010b.
- Z. Dodin and T. Elperin. On the collision rate of particles in turbulent flow with gravity. *Physics of Fluids*, 14(8):2921–2924, 2002.
- T. Hagemeier, M. Hartmann, and D. Thévenin. Practice in vehicle soiling investigation: a Review. *International Journal of Multiphase Flow*, 2011. accepted for publication.
- R. Kapulla, M. Trautmann, A.H. Sanchez, S.C. Zaragoza, C. Häfeli, and S. Güntay. Droplet size distribution measurements using phase-Doppler anemometry and shadowgraphy: Quantitative comparison. In D. Doppeide, H. Müller, V. Strunck, B. Ruck, and A. Leder, editors, *Lasermethoden in der Strömungsmesstechnik*, pages 27.1–6, Rostock, Germany, GALA, 2007.
- M. Pinsky, A. Khain, and H. Krugliak. Collisions of cloud droplets in a turbulent flow. part v: Application of detailed tables of turbulent collision rate enhancement to simulation of droplet spectra evolution. *Journal of the Atmospheric Sciences*, 65(2):357374, 2008.
- R. A. Shaw, W. C. Reade, L. R. Collins, and J. Verlinde. Preferential concentration of cloud droplets by turbulence: Effects on the early evolution of cumulus cloud droplet spectra. *Journal of the Atmospheric Sciences*, 55(11):1965–1976, 1998.
- J. J. E. Williams and R. I. Crane. Particle collision rate in turbulent flow. *International Journal of Multiphase Flow*, 9:421, 1983.